Heliyon 9 (2023) e22553

Contents lists available at ScienceDirect

Heliyon

journal homepage: www.cell.com/heliyon

On the optimized energy transport rate of magnetized micropolar fluid via ternary hybrid ferro-nanosolids: A numerical report

Mohammed Z. Swalmeh [a], Firas A. Alwawi [b], A.A. Altawallbeh [c], Kohilavani Naganthran [d,e,*], Ishak Hashim [f,g]

[a] Faculty of Arts and Sciences, Aqaba University of Technology, Aqaba, 77110, Jordan
[b] Department of Mathematics, College of Sciences and Humanities in Al-Kharj, Prince Sattam Bin Abdulaziz University, Al-Kharj, 11942, Saudi Arabia
[c] Department of Mathematics, School of Basic and Marine Sciences. the University of Jordan, 77110, Aqaba, Jordan
[d] Institute of Mathematical Sciences, Faculty of Science, Universiti Malaya, 50603 Kuala Lumpur, Malaysia
[e] Center for Data Analytics, Consultancy and Services, Faculty of Science, Universiti Malaya, 50603 Kuala Lumpur, Malaysia
[f] Department of Mathematical Sciences, Faculty of Science and Technology, Universiti Kebangsaan Malaysia, 43600, UKM, Bangi, Selangor, Malaysia
[g] Nonlinear Dynamics Research Center (NDRC), Ajman University, Ajman P.O. Box 346, United Arab Emirates

ARTICLE INFO

Keywords:
Ferro ternary hybrid-nanofluid
Mixed convection
Micropolar fluid
Spherical object
Lorentz force

ABSTRACT

In the current era, a chemical, industrial, or production process may not be devoid of heat transfer processes through fluids. This is seen in evaporators, distillation units, dryers, reactors, refrigeration and air conditioning systems, and others. On the other hand, the micropolar model effectively simulates microstructured fluids like animal blood, polymeric suspensions, and crystal fluid, paving the way for new potential applications based mainly on complex fluids. This investigation attempts to figure out and predict the thermal behavior of a polar fluid in motion across a solid sphere while considering the Lorentz force and mixed convection. To support the original fluid's thermophysical characteristics, two types of ternary hybrid ferro-nanomaterials are used. The problem is modelled using a single-phase model. Then, using the Keller box approximation, a numerical finding is obtained. The study reveals that Increasing the volume fraction of the ternary hybrid nonsolid results in optimized values of Nusselt number, velocity, and temperature. The presence of Lorentz forces effectively mitigates flow strength, skin friction, and energy transfer rate. The mixed convection factor contributes significantly to enhanced energy transfer and improved flow scenarios. For maximum heat transfer efficiency, employing Fe_3O_4–Cu–SiO_2 is recommended over Fe_3O_4–Al_2O_3–TiO_2.

1. Introduction

The micropolar theory of fluids is an essential and simplified generalization of the classical Navier-Stokes model, which was presented by A.C. Eringen [1,2] and has become one of the most preferred models in many theoretical studies and applications. This expanded model has effectively simulated the behavior of microstructured fluids like animal blood, polymeric suspensions, and crystal fluid, to name a few. It also paved the way for a slew of new potential applications based mainly on complex fluids. Recently, Nazar

* Corresponding author. Institute of Mathematical Sciences, Faculty of Science, Universiti Malaya, 50603, Kuala Lumpur, Malaysia.
E-mail address: kohi@um.edu.my (K. Naganthran).

https://doi.org/10.1016/j.heliyon.2023.e22553
Received 9 July 2023; Received in revised form 4 October 2023; Accepted 15 November 2023
Available online 20 November 2023

et al. [3–5] conducted a numerical simulation of the behavior of a polar fluid flowing over a sphere, taking into account combined and free convection. Cheng [6] looked into the transmission of mass and energy in a polar fluid moving around a spherical surface. Salleh et al. [7] examined the energy transport characteristics of micropolar liquid moving over a sphere considering Newtonian heating. Roy et al. [8] published a paper on the unsteady MHD-free and forced convection of polar liquid over a permeable spherical object. Swalmeh et al. [9] and Alzgool et al. [10] have employed the Tiwari-Das nanoliquid model to extend some previous investigations on heat transport via micropolar liquid flowing over a spherical object. Free convection was studied by EL-Kabeir et al. [11] in the case of ferro-micropolar liquid moving around a radiative isoflux spherical surface.

In the current era, a chemical, industrial, or production process may not be devoid of heat transfer processes through fluids. This can be seen in a wide variety of devices and equipment, such as evaporators, distillation units, dryers, reactors, refrigeration and air conditioning devices, and many others. One of the main challenges for the work of these devices is that they must transfer heat at the required rate or provide adequate insulation. To achieve these ends, researchers devised several methods, among the most effective of which was the one proposed by Choi and Eastman [12]. They focused on improving the thermal fluid's capabilities based on nanoparticles. These nanoparticles were effective in reinforcing the thermal conductivity of the host liquid, and their nanoscale size contributed to overcoming prevailing problems such as clogging and instability. Many subsequent experimental and numerical publications emphasized the enhancement of the thermal features of the host liquid by nanoparticles, like density and viscosity, heat capacity, thermal diffusivity, and so on [13–17]. Two types of nanoparticles have been commonly used: metallic nanoparticles, which give the host liquid high thermal conductivity but have lower stability, and non-metallic nanoparticles, which have high stability but give the host fluid relatively lower thermal conductivity [18–21]. Therefore, the researchers had to choose between good stability and high thermal conductivity. This in itself is a problem, as one of the two options does not meet the growing application requirements. One of the suggestions is to synthesize hybrid nanoparticles, which are a new generation of nanoparticles with integrated physical and chemical properties [22–25]. Recently, a large group of scientists examined the thermal properties of these distinctive nanoparticles and the extent of their effect on the host fluids through mathematical simulations. Jamaludin et al. [26] explored numerically the magneto-convective flow of a hybrid nanofluid across a permeable stretching body with a heat source. Nasir et al. [27] investigated numerically the effect of hall current on time-dependent convection flow produced by a hybrid nanoliquid on a whirling spherical surface. Using the Chebyshev pseudo spectral differentiation matrix technique, Aly et al. [28] investigated a radiative combined convective flow of hybrid nanoliquid over a nonlinearly stretching body. Alwawi et al. [29] explored the thermal behavior of Williamson hybrid nanoliquid flowing about a cylindrical surface, considering Lorentz force and radiation impact. Some scholars have greatly contributed to hybrid nanofluid studies by analyzing various approaches [30–36]. In the last three years, an upgraded generation of nanoparticles has appeared, termed "ternary hybrid nanoparticles." It is created by fusing three solid nanomaterials. This generation outperforms the previous two generations in terms of thermal performance, meets researcher expectations, and is expected to satisfy the future demands of applications [37–40]. Several numerical studies have shed light on this advanced type of nanoparticle. Khan et al. [41] examined the impact of ohmic heating on the flow of a tri-hybrid nanoliquid with viscous dissipation and suction. They found that higher amounts of nanosolids in the host liquid increased the rate of energy transport. Manjunatha et al. [42] examined the thermal performance of a magnetized tri-hybrid nanofluid with a chemical reaction towards an extending surface. They employed the RKF-45 approximation to obtain a numerical solution for their issue. Algehyne et al. [43] looked into the thermal behavior in porous media of pseudo-plastic tri-hybrid nanofluid moving over a surface using non-Fourier laws. Animasaun et al. [44] explored the effect of density, magnetic variability, and heat sink/source on the characteristic flow of ternary hybrid nanoliquid under a heated surface. See also [45–48]. Ferro-nanomaterials are ultrafine particles that respond strongly to magnetic fields. These magnetic nanomaterials are typically made of hematite, ferrite, magnetite, iron, iron oxide, etc. These particles possess unique properties that qualify them to be the best choice in a wide range of engineering applications, particularly those aimed at improving energy transmission [49,50]. The current study relies on two types of ferro ternary hybrid nanoparticles, Fe_3O_4–Al_2O_3–TiO_2 and Fe_3O_4–Cu–SiO_2, to explore the extent of the improvement in ethylene glycol-water's thermal performance when reinforced with these unique nanoparticles.

In practice, mixed convection is essential throughout many engineering and manufacturing application fields. It is fully evident in the refrigeration of electronic devices and nuclear reactors, in addition to food manufacturing and solar energy systems [51,52]. The magnetic field has the ability to induce Lorentz forces in a flowing fluid, slowing it down and increasing the fluid's temperature and concentration. Consequently, incorporating the magnetic field has the potential to delay boundary layer separation. Many researchers looked into mixed convection in the presence of induced Lorentz forces. Especially in the boundary layer flow case. Nasir et al. [53] provided a novel investigation employing computational simulation to explore the mangntohydrodynamic three dimensional rotating flow of nanoliquid across a radiative stretching sheet. Alsagri et al. [54] numerically looked into the energy transmission and MHD finite film flow of CNT-human blood nanoliquids over a stretchable upright cylinder. Nasir et al. [55] examined the time-dependent free convection stagnation point flow of nanoliquid past an EMHD Riga plate in motion with a radiation impact. Swalmeh et al. [56] conducted a numerical investigation of the radiation's impact on MHD mixed convection in polar nanoliquid around a spherical body. Alwawi et al. [29,57] looked at how the Lorentz force affects the flow of Casson and hybrid Williamson nanoliquids around a cylinder. They took into account the combined convection. On the other hand, the boundary layer flow on a solid sphere is of great significance in numerous industrial applications, showcasing its versatility and practicality. One notable application is in spherical storage tanks, where understanding the boundary layer flow over a sphere aids in optimizing heat transfer and maintaining uniform temperatures within the tank. In the realm of automotive engineering, the boundary layer flow on a solid sphere is relevant to turbocharged ball bearings, which require efficient lubrication and reduced friction. The packed beds in chemical reactors and distillation processes also benefit from an understanding of boundary layer flow over a sphere, as it influences mass and heat transfer efficiency. Additionally, electronic components that are nearly spherical, such as microspheres or sphere-shaped heat sinks, rely on the control and management of boundary layer flow over a sphere for effective cooling and heat dissipation [58–60].

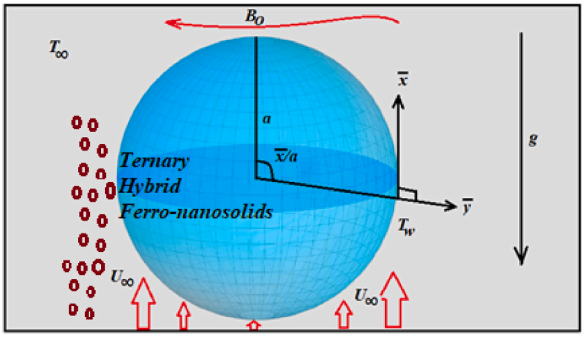

Fig. 1. Physical schematic and coordinate system.

The current study is of vital significance as it allows a detailed illustration of the combined convection and heat transfer of the fluids that phenomena have experienced in modern practical engineering applications. On the other hand, this finding includes ternary hybrid nanofluids, which contain a combination of three different nanoparticles. This investigation presents a new extent to the examination as it studies the influences of combined convection with the addition of micropolar ternary hybrid nanofluid features. Furthermore, the research takes into account the impacts of a magnetic domain on the boundary layer flow; hence, the magnetic parameter is implied, which qualifies it for the study of the associated interactions between the heat transfer, the magnetohydrodynamic characteristics, and micropolar ternary hybrid nanofluids. Comprehending these above relations is an important optimization of industrial and engineering systems. Based on the above, a mathematical model is developed that includes the governing dimensional equations for the combined convection boundary layer flow in the presence of a magnetic effect and takes into account the micropolar ternary hybrid nanofluids. Employing the appropriate transformations, proceed to obtain partial differential equations and solve these equations using an effective numerical method, namely the Keller box method. The acquired linear system, from the Keller box method, is programmed using the MATLAB program, obtaining accurate numerical results, comparing them with previous literature, and going directly to obtain new outcomes through tables and figures.

2. Formulation of the problem

Consider that we have combined (mixed) convection in a micropolar ternary hybrid nanofluid moving around a solid sphere of radius a and a constant surface temperature T_w boundary conditions. In addition, it is assumed that there is an external magnetic field of strength B_0. The suggested direction flow is perpendicular to the magnetic field direction as shown in Fig. 1. Two kinds of ternary hybrid ferro-nanosolids are carried into consideration, Fe_3O_4–Al_2O_3–TiO_2 and Fe_3O_4–Cu–SiO_2, which are suspended in H_2O-EG 50 %. The circumference of the solid sphere is measured by orthogonal axes, namely x and y, starting from the lower stagnation point $x \approx 0$. T_∞ is the surrounding temperature, g is the gravitational force, and U_∞ is the free stream velocity.

Counting on the mentioned assumptions, under Boussinesq's two-dimensional incompressible model and based on prior literature that considered the combined (mixed) convection in microploar model [3], ternary hybrid nanofluid [61], and magnetic force [62], the mathematical model is:

$$\frac{\partial \overline{r}\overline{v}}{\partial \overline{x}} + \frac{\partial \overline{r}\overline{w}}{\partial \overline{y}} = 0, \tag{1}$$

$$\rho_{thnf}\left(\overline{v}\,\frac{\partial \overline{v}}{\partial \overline{x}} + \overline{w}\frac{\partial \overline{v}}{\partial \overline{y}}\right) = \left(\overline{v}_e\frac{\partial \overline{v}_e}{\partial \overline{x}} + \frac{\sigma_{thnf}B_0^2 a}{U_\infty}v_e\right) + \left(\mu_{thnf} + \kappa\right)\left(\frac{\partial^2 \overline{v}}{\partial \overline{y}^2}\right) +$$

$$\left(\beta_{thnf}\right)g(T - T_\infty)sin\frac{\overline{x}}{a} + \kappa\left(\frac{\partial \overline{G}}{\partial \overline{y}}\right) - \sigma_{thnf}B_0^2\overline{w}, \tag{2}$$

$$\overline{v}\,\frac{\partial T}{\partial \overline{x}} + \overline{w}\,\frac{\partial T}{\partial \overline{y}} = \alpha_{thnf}\left(\frac{\partial^2 \overline{T}}{\partial \overline{y}^2}\right), \tag{3}$$

$$\rho_{thnf}j\left(\overline{v}\,\frac{\partial \overline{G}}{\partial \overline{x}} + \overline{w}\frac{\partial \overline{G}}{\partial \overline{y}}\right) = \varphi_{thnf}\left(\frac{\partial^2 \overline{G}}{\partial \overline{y}^2}\right) + \kappa\left(-2\overline{G} + \frac{\partial \overline{v}}{\partial \overline{y}}\right). \tag{4}$$

The constant wall temperature boundary conditions are:

$$\overline{v} = \overline{w} = 0, T = T_w, \overline{G} = -(1/2)\frac{\partial \overline{v}}{\partial \overline{y}}, \text{ as } \overline{y} = 0,$$

$$\overline{v} \to \overline{v}_e(\overline{x}), \overline{w} \to 0, T \to T_\infty, \overline{G} \to 0, \text{ as } \overline{y} \to \infty, \tag{5}$$

Table 1
Nanoliquid thermophysical characteristics [47,61].

$(\mu)_{thnf} = \frac{\mu_f}{(1-\chi_A)^{2.5}(1-\chi_B)^{2.5}(1-\chi_C)^{2.5}}$
$(\rho c_p)_{thnf} = (1-\chi_A)[(1-\chi_B)\,[(1-\chi_C)$
$(\rho)_{thnf} = (1-\chi_A)[(1-\chi_B)\,[(1-\chi_C)\rho_f + \chi_C\rho_C] + \chi_B\rho_B] + \chi_A\rho_A$
$\varphi_{thnf} = (\mu_{thnf} + \kappa/2)j$, $(\alpha)_{thnf} = \frac{k_{thnf}}{(\rho c_p)_{thnf}}$,
$\frac{k_{thnf}}{k_{hnf}} = \frac{(k_A+2k_{hnf})-2\chi_A(k_{hnf}-k_A)}{(k_A+2k_{hnf})+\chi_A(k_{hnf}-k_A)}$,
$\frac{k_{hnf}}{k_{nf}} = \frac{(k_B+2k_{nf})-2\chi_B(k_{nf}-k_B)}{(k_B+2k_{nf})+\chi_B(k_{nf}-k_B)}$,
$\frac{k_{nf}}{k_f} = \frac{(k_C+2k_f)-2\chi_C(k_f-k_C)}{(k_C+2k_f)+\chi_C(k_f-k_C)}$
$\sigma_{thnf} = \left[1 + \frac{3((\sigma_A/\sigma_{hnf})-1)\,\chi_A}{((\sigma_A/\sigma_{hnf})+2) - \chi_A\,((\sigma_A/\sigma_{hnf})-1)}\right]\sigma_{hnf}$,
$\sigma_{hnf} = \left[1 + \frac{3((\sigma_B/\sigma_{nf})-1)\,\chi_B}{((\sigma_B/\sigma_{nf})+2) - \chi_B\,((\sigma_B/\sigma_{nf})-1)}\right]\sigma_{nf}$,
$\sigma_{nf} = \left[1 + \frac{3((\sigma_C/\sigma_f)-1)\,\chi_C}{((\sigma_C/\sigma_f)+2) - \chi_C\,((\sigma_C/\sigma_f)-1)}\right]\sigma_f$

where $\overline{v}$ and $\overline{w}$ are velocity components in $\overline{x}$ and $\overline{y}$ orientations, respectively. $j = av_f/U_\infty$, $\varphi_{thnf} = j(\mu_{thnf} + \kappa/2)$, $j = av_f/U_\infty$, $\alpha_{thnf} = k_{thnf}/(\rho Cp)_{thnf}$ and $\overline{v}_e = (3/2)U_\infty \sin(\overline{x}/a)$ symbolize the micro-inertia density, spin gradient viscosity, thermal diffusivity, and velocity of external flow, respectively. The subscript indicates the ternary hybrid nanoliquid. Mono, hyprid, and tri-hybrid nanoliquids' thermophysical properties are offered in Table 1.

The subscripts *A, B,* and *C* represent specific nanoparticles, as: $A = Fe_3O_4$, $B =$ Cu or Al_2O_3, $C = SiO_2$ or TiO_2.

The dimensionless variables used in this investigation are defined as:

$$x = \frac{\overline{x}}{a}, y = (Re)^{(1/2)}a^{-1}\overline{y}, r(x) = \overline{r}(\overline{x})/a\ \theta = k_f(aq_w)^{-1}Re^{1/2}(T - T_\infty),$$

$$v = \frac{\overline{v}}{U_\infty}, w = (Re)^{(1/2)}a^{-1}\overline{w}, G = aU_\infty^{-1}Re^{-1}\,\overline{G}, v_e = \overline{v}_e U_\infty^{-1}. \tag{6}$$

$Re = U_\infty a v_f^{-1}$ symbolize the Reynolds number. Substituting the non-dimensional variables (6) and using the physical characteristics, in Table 1, the above equations (1)–(4) can be obtained in a non-dimensional form as:

$$\frac{\partial(rv)}{\partial x} + \frac{\partial(rw)}{\partial y} = 0, \tag{7}$$

$$v\frac{\partial v}{\partial x} + w\frac{\partial v}{\partial y} = v_e\frac{\partial v_e}{\partial x} + \frac{\rho_f}{\rho_{thnf}}\left[\frac{1}{(1-\chi_A)^{2.5}(1-\chi_B)^{2.5}(1-\chi_C)^{2.5}} + K\right]\left(\frac{\partial^2 v}{\partial y^2}\right)$$
$$+\left(\frac{1}{\rho_{thnf}}(1-\chi_A)\left[(1-\chi_B)\left[(1-\chi_C) + \chi_C\frac{\beta_C}{\beta_f}\right] + \chi_B\frac{\beta_B}{\beta_f}\right] + \chi_A\frac{\beta_A}{\beta_f}\right)\lambda\theta\sin x$$
$$+\frac{\rho_f}{\rho_{thnf}}K\frac{\partial G}{\partial y} + \frac{\rho_f}{\rho_{thnf}}\frac{\sigma_{thnf}}{\sigma_f}M(v_e - w), \tag{8}$$

$$v\frac{\partial\theta}{\partial x} + w\frac{\partial\theta}{\partial y} = \frac{1}{\mathrm{Pr}}\left(\frac{k_{thnf}/k_f}{(1-\chi_A)\left[(1-\chi_B)\left[(1-\chi_C) + \chi_C\frac{(\rho c_p)_C}{(\rho c_p)_f}\right] + \chi_B\frac{(\rho c_p)_B}{(\rho c_p)_f}\right] + \chi_A\frac{(\rho c_p)_A}{(\rho c_p)_f}}\right)\left(\frac{\partial^2\theta}{\partial y^2}\right), \tag{9}$$

$$v\frac{\partial G}{\partial x} + v\frac{\partial G}{\partial y} = -\frac{\rho_f}{\rho_{thnf}}K\left(2G + \frac{\partial w}{\partial y}\right) + \frac{\rho_f}{\rho_{thnf}}\left(\frac{1}{(1-\chi_A)^{2.5}(1-\chi_B)^{2.5}(1-\chi_C)^{2.5}} + \frac{K}{2}\right)\left(\frac{\partial^2 G}{\partial y^2}\right), \tag{10}$$

subject to:

$$v = w = 0, \theta = 1, G = -(1/2)\frac{\partial v}{\partial y} \text{ as } y = 0,$$

$$v \to v_e(x), \theta, G \to 0 \text{ as } y \to \infty, \tag{11}$$

wherein $\lambda = Gr/Re^2$ is the combined convection factor, $Gr = g\beta(T_w - T_\infty)a^2/\nu_f^2$ is the Grashof number, and $Pr = \nu_f/\alpha_f$ is called the Prandtl number. As well as the magnetic parameter is given as $M = \rho_f B_0^2 a^2 G^{-1/2}/\rho_f \nu_f$, $K = k/\mu_f$ is the micropolar parameter and χ is the nanoparticle volume fraction parameter. The stream transformation ψ is expressed mathematically as:

$$v = \frac{\partial \psi}{\partial x} \text{ and } w = \frac{\partial \psi}{\partial x}, \tag{12a}$$

Using the following variables:

$$\psi = xf(x,y), \theta = \theta(x,y), G = x\,G(x,y). \tag{12b}$$

Replacing (12) into (7)–(11) to get the following PDEs:

$$\frac{\rho_f}{\rho_{thnf}}\left[\frac{1}{(1-\chi_A)^{2.5}(1-\chi_B)^{2.5}(1-\chi_C)^{2.5}} + K\right]\frac{\partial^3 f}{\partial y^3} + (1 + x\cot x)f\frac{\partial^2 f}{\partial y^2} - \left(\frac{\partial f}{\partial y}\right)^2$$

$$+\left(\frac{1}{\rho_{thnf}}(1-\chi_A)\left[(1-\chi_B)\left[(1-\chi_C) + \chi_C\frac{\beta_C}{\beta_f}\right] + \chi_B\frac{\beta_B}{\beta_f}\right] + \chi_A\frac{\beta_A}{\beta_f}\right)\lambda\theta\frac{\sin x}{x}$$

$$+\frac{9\sin x\cos x}{4x} + \frac{\rho_f}{\rho_{thnf}}K\left(\frac{\partial G}{\partial y}\right) + \frac{\rho_f}{\rho_{thnf}}\frac{\sigma_{thnf}}{\sigma_f}M\left(\frac{\sin x}{x} - \frac{\partial f}{\partial y}\right) = x\left(\frac{\partial f}{\partial y}\frac{\partial^2 f}{\partial x \partial y} - \frac{\partial f}{\partial x}\frac{\partial^2 f}{\partial y^2}\right), \tag{13}$$

$$\frac{1}{\Pr}\left(\frac{k_{thnf}/k_f}{(1-\chi_A)\left[(1-\chi_B)\left[(1-\chi_C) + \chi_C\frac{(\rho c_p)_C}{(\rho c_p)_f}\right] + \chi_B\frac{(\rho c_p)_B}{(\rho c_p)_f}\right] + \chi_A\frac{(\rho c_p)_A}{(\rho c_p)_f}}\right)\left(\frac{\partial^2 \theta}{\partial y^2}\right) + f\frac{\partial \theta}{\partial y} = x\left(\frac{\partial f}{\partial y}\frac{\partial \theta}{\partial x} - \frac{\partial f}{\partial x}\frac{\partial \theta}{\partial y}\right), \tag{14}$$

$$\frac{\rho_f}{\rho_{thnf}}\left(\frac{1}{(1-\chi_A)^{2.5}(1-\chi_B)^{2.5}(1-\chi_C)^{2.5}} + \frac{K}{2}\right)\left(\frac{\partial^2 G}{\partial y^2}\right) + f\frac{\partial G}{\partial y} - \frac{\partial f}{\partial y}G$$

$$-\frac{\rho_f}{\rho_{nf}}K\left(2G + \frac{\partial^2 f}{\partial \omega^2}\right) = x\left(\frac{\partial f}{\partial y}\frac{\partial G}{\partial x} - \frac{\partial f}{\partial x}\frac{\partial G}{\partial y}\right), \tag{15}$$

subject to:

$$f = \frac{\partial f}{\partial y} = 0, \theta = 1, G = -(1/2)\frac{\partial^2 f}{\partial y^2}, \text{ as } y = 0,$$

$$\frac{\partial f}{\partial y} \to (3/2)\frac{\sin x}{x}, \theta \to 0, G \to 0, \text{ as } y \to \infty. \tag{16}$$

Moreover, equations (13)–(16) at the stagnation point ($x \approx 0$) are written as follows:

$$\frac{\rho_f}{\rho_{thnf}}\left[\frac{1}{(1-\chi_A)^{2.5}(1-\chi_B)^{2.5}(1-\chi_C)^{2.5}} + K\right]f''' + 2ff'' - (f')^2$$

$$+\left(\frac{1}{\rho_{thnf}}(1-\chi_A)\left[(1-\chi_B)\left[(1-\chi_C) + \chi_C\frac{\beta_C}{\beta_f}\right] + \chi_B\frac{\beta_B}{\beta_f}\right] + \chi_A\frac{\beta_A}{\beta_f}\right)\lambda\theta$$

$$+\frac{9}{4} + \frac{\rho_f}{\rho_{thnf}}K\left(\frac{\partial G}{\partial y}\right) + \frac{\rho_f}{\rho_{thnf}}\frac{\sigma_{thnf}}{\sigma_f}M(1 - f') = 0, \tag{17}$$

$$\frac{1}{\Pr}\left(\frac{k_{thnf}/k_f}{(1-\chi_A)\left[(1-\chi_B)\left[(1-\chi_C) + \chi_C\frac{(\rho c_p)_C}{(\rho c_p)_f}\right] + \chi_B\frac{(\rho c_p)_B}{(\rho c_p)_f}\right] + \chi_A\frac{(\rho c_p)_A}{(\rho c_p)_f}}\right)\theta'' + f\theta' = 0, \tag{18}$$

$$\frac{\rho_f}{\rho_{thnf}}\left(\frac{1}{(1-\chi_A)^{2.5}(1-\chi_B)^{2.5}(1-\chi_C)^{2.5}}+\frac{K}{2}\right)(G^{''})+fh^{'}-f^{'}G-\frac{\rho_f}{\rho_{thnf}}K(2G+f^{''})=0. \tag{19}$$

Under the converted boundary conditions:

$$f(0)=f^{'}(0)=0,\theta(0)=1,G(0)=-(1/2)f^{''}(0),\ \text{as } y\to 0,$$

$$f^{'}\to 3/2,\theta\to 0,G\to 0,\ \text{as } y\to\infty. \tag{20}$$

The local skin friction coefficient Cf and the local Nusselt number *Nu* are expressed as [63]:

$$C_f=Re^{-1/2}\left[\frac{1}{(1-\chi_A)^{2.5}(1-\chi_B)^{2.5}(1-\chi_C)^{2.5}}+\frac{K}{2}\right]x\frac{\partial^2 f}{\partial\omega^2}\ |_{y=0},$$

$$Nu=Re^{1/2}\frac{k_{thnf}}{k_f}\left(\frac{\partial\theta}{\partial y}\right)|_{y=0}. \tag{21}$$

Here, the Keller box numerical scheme procedures were relied upon to explore accurate numerical outcomes for the above partial differential equations (PDEs). Firstly, it can be introduced the following independent variables to reduce PDEs to third-order by the finite difference scheme:

$$f^{'}=v,v^{'}=w,G^{'}=g,\theta^{'}=s, \tag{22}$$

equations (13)–(16) transformed to the finite difference equations as:

$$\frac{\rho_f}{\rho_{thnf}}\left[\frac{1}{(1-\chi_A)^{2.5}(1-\chi_B)^{2.5}(1-\chi_C)^{2.5}}+K\right]v^{'}+(1+x\cot x)fw-v^2$$

$$+\left(\frac{1}{\rho_{thnf}}(1-\chi_A)\left[(1-\chi_B)\left[(1-\chi_C)+\chi_C\frac{\beta_C}{\beta_f}\right]+\chi_B\frac{\beta_B}{\beta_f}\right]+\chi_A\frac{\beta_A}{\beta_f}\right)\lambda\theta\frac{\sin x}{x}$$

$$+\frac{9\sin x\cos x}{4x}+\frac{\rho_f}{\rho_{thnf}}Kg+\frac{\rho_f}{\rho_{thnf}}\frac{\sigma_{thnf}}{\sigma_f}M\left(\frac{\sin x}{x}-\frac{\partial f}{\partial y}\right)=x\left(v\frac{\partial u}{\partial x}-w\frac{\partial f}{\partial x}\right), \tag{23}$$

$$\frac{1}{\mathrm{Pr}}\left(\frac{k_{thnf}/k_f}{(1-\chi_A)\left[(1-\chi_B)\left[(1-\chi_C)+\chi_C\frac{(\rho c_p)_C}{(\rho c_p)_f}\right]+\chi_B\frac{(\rho c_p)_B}{(\rho c_p)_f}\right]+\chi_A\frac{(\rho c_p)_A}{(\rho c_p)_f}}\right)s^{'}+fs=x\left(v\frac{\partial\theta}{\partial x}-s\frac{\partial f}{\partial x}\right), \tag{24}$$

$$\frac{\rho_f}{\rho_{thnf}}\left(\frac{1}{(1-\chi_A)^{2.5}(1-\chi_B)^{2.5}(1-\chi_C)^{2.5}}+\frac{K}{2}\right)g^{'}+fg-vG-\frac{\rho_f}{\rho_{nf}}K(2G+w)=x\left(v\frac{\partial G}{\partial x}-g\frac{\partial f}{\partial x}\right), \tag{25}$$

subject to:

$$f(x,0)=0,v(x,0)=0,\theta(x,0)=1,G(x,0)=-(1/2)\,w(x,0),$$

$$v(x,\infty)=(3/2),\theta(x,\infty)=0,G(x,\infty)=0, \tag{26}$$

where the primes indicate the derivative of variable *y*.

3. Numerical approximation and validation

In such works of applied mathematics, engineering, and physics, sometimes a special system of partial differential equations arises repeatedly. These equations have been widely studied, and articles have been documented on the characteristics of their numerical approximate solutions and how to solve them. This is one of the studies that included a special system of partial differential equations that needed a numerical method to obtain accurate results for their solutions. The Keller box technique is one such well-known, effective, accurate, and flexible method that was used for solving the partial differential equations in this study, which involves the finite difference method Reduce the transformed partial differential equations (17)–(20) to a first-order system; rewrite the attained system as the difference equations using central differences. Moreover, linearize the difference equations into a linear system of

Table 2
Comparison the present results of Cf with previous literature.

x	λ							
	−3		−1		0		1	
	Nazar et al. [3]	Present work	Nazar et al. [3]	Present work	Nazar et al. [3]	Present work	Nazar et al. [3]	Present work
0°	0.0000	0.0000	0.0000	0.0000	0.0000	0.0000	0.0000	0.0000
10°	0.1806	0.1822	0.3438	0.3790	0.4160	0.4583	0.4843	0.4884
20°	0.3261	0.3281	0.6564	0.6590	0.8014	0.8065	0.9380	0.9618
30°	0.4024	0.4092	0.9098	1.0067	1.1284	1.1307	1.3335	1.3571
40°	0.3704	0.3777	1.0790	1.1824	1.3733	1.3811	1.6471	1.6487
50°			1.1434	1.1449	1.5172	1.5208	1.8607	1.8642
60°			1.0866	1.0898	1.4577	1.4617	1.9627	1.9305
70°			0.8929	0.9090	1.4583	1.4597	1.9486	1.9524
80°			0.5280	0.5663	1.2480	1.2499	1.8216	1.8273
90°					0.9154	0.9182	1.5315	1.5392
100°					0.4308	0.4326	1.2732	1.2764
110°							0.8831	0.8883
120°							0.4420	0.4496

Table 3
Comparison the present results of *Nu* with previous literature.

x	λ							
	−3		−1		0		1	
	Nazar et al. [3]	Present work	Nazar et al. [3]	Present work	Nazar et al. [3]	Present work	Nazar et al. [3]	Present work
0°	0.7108	0.7217	0.7870	0.8221	0.8162	0.8173	0.8463	0.8541
10°	0.7040	0.7058	0.7818	0.7848	0.8112	0.8118	0.8371	0.8440
20°	0.6845	0.6884	0.7669	0.7672	0.7974	0.8254	0.8239	0.8288
30°	0.6507	0.6538	0.7422	0.7501	0.7746	0.7776	0.8024	0.8064
40°	0.5977	0.6106	0.7076	0.7124	0.7429	0.7473	0.7725	0.7773
50°			0.6624	0.6672	0.7022	0.7062	0.7345	0.7352
60°			0.6055	0.6110	0.6525	0.6617	0.6887	0.6913
70°			0.5224	0.5234	0.5934	0.6026	0.6352	0.6391
80°			0.4342	0.4358	0.5236	0.5267	0.5742	0.5781
90°					0.4398	0.4419	0.5060	0.5102
100°					0.3263	0.3317	0.4304	0.4315
110°							0.3458	0.3464
120°							0.2442	0.2462

Table 4
Thermo-physical characteristics of the original liquid and considered nanomaterials [30,56,66,67].

Thermo-Physical feature	$H_2O + EG50$ %	Cu	Fe_3O_4	SiO_2	Al_2O_3	TiO_2
C_p $(J/kg\ K)$	3288	235	670	717	765	686.2
$\beta \times 10^{-5}(K^{-1})$	0.00341	1.89	20.6	28	0.85	0.9
ρ (kg/m^3)	1056	10,500	5180	1800	3970	4250
K $(W/m\ K)$	0.425	429	80.4	5000	40	8.9528
$\sigma(S/m)$	0.00509	6.3×10^7	1.12×10^5	6.3×10^7	3.5×10^7	2.6×10^6
Pr	29.86	…	…	…	…	

equations using Newton's method. Formulate the linear system as a matrix and a vector. As a last step, we'll solve the matrix-vector form using the block tri-diagonal elimination method to attain an accurate approximation of solutions [64,65]. Final numerical results were visualized as graphs and tabulated using the MATLAB programmer. In this type of numerical simulation study, and when programming the linear system of equations that resulted from the Keller box scheme, via MATLAB code, to get accurate numerical results, the convergence criterion must be determined and explained in detail. Thus, we need to determine some explicit calculations: the proper steps size Δx and Δy, also the boundary layer thickness y_∞, in the present investigation y_∞ suitably valued from 0.6 to 4.5, to bring the boundary layer convergence. Once the appropriate value of y_∞ is fixed, we select the step size $\Delta x = 0.01$ and step size $\Delta y = 0.02$, which are timely for acquiring valid and accurate approximate numerical results. These values are employed to obtain numerical outcomes nearly consistent with prior literature, as displayed in Tables 2 and 3. The calculations are repeated until convergence criteria are achieved. The new results of this study for a special case ($-3 \leq \lambda \leq 1, K = M = \psi = 0$, Pr $= 0.7$) are compared with previous literature [3] for local skin friction and local Nusselt number in both states of flow (aiding flow $\lambda > 0$, and opposing flow $\lambda < 0$) in order to ensure the accuracy of the current method, as shown in Tables 2 and 3 It is worth mentioning that the minor differences in

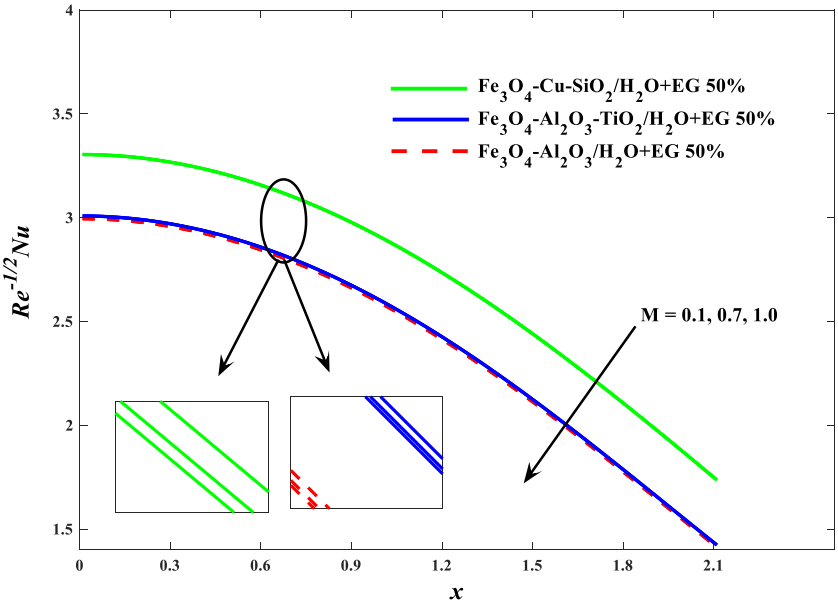

Fig. 2. $Re^{-1/2}Nu$ impression to M influence, at $\chi_{ABC}= 0.05, \lambda= 2$ and $K= 2$.

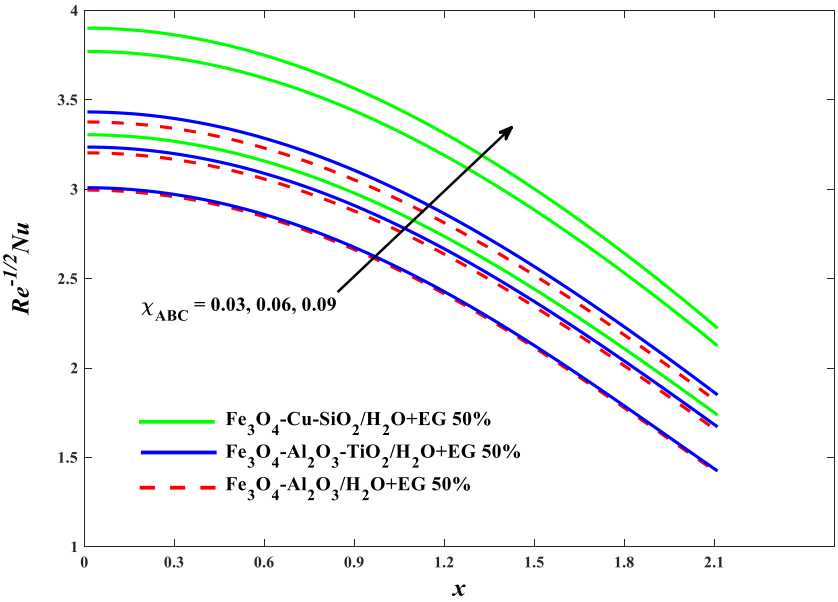

Fig. 3. $Re^{-1/2}Nu$ impression to χ_{ABC} influence, at $M= 0.5, \lambda= 2$ and $K= 2$.

Tables 2 and 3, are caused by the different boundary layer thickness values that are entered into the MATLAB program. So, every researcher enters the different larger boundary layer thickness values to get smooth curves and more accurate outcomes. It is obvious that our results achieved excellent compatibility. Table 4 presents the thermo-physical characteristics of the utilized nanosolids and the original liquid.

4. Results and discussions

This portion describes and analyses the perceptions and trends of physical groups specifically linked to heat transport, in addition to their interaction when increasing the values of the volume fraction, the micropolar factor, the combined convection factor, and the magnetic factor. Fig. 2 depicts the Nusselt number trending in the availability of a rising magnetic parameter with other parameters held fixed. The Nusselt number evidently declines as the magnetic value increases. This is an expected pattern of Nusselt number since

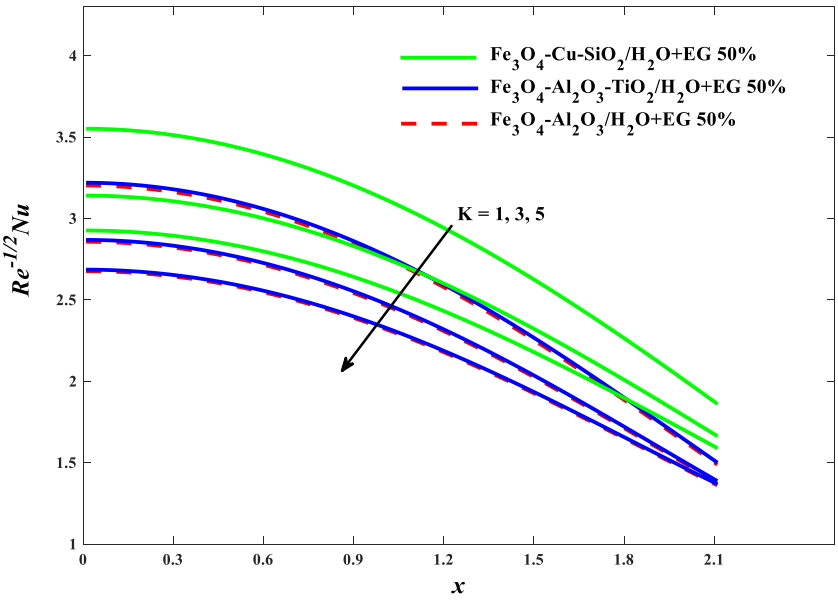

Fig. 4. $Re^{-1/2}Nu$ impression to K influence, at $\chi_{ABC}= 0.03, M= 0.5$ and $K= 2$.

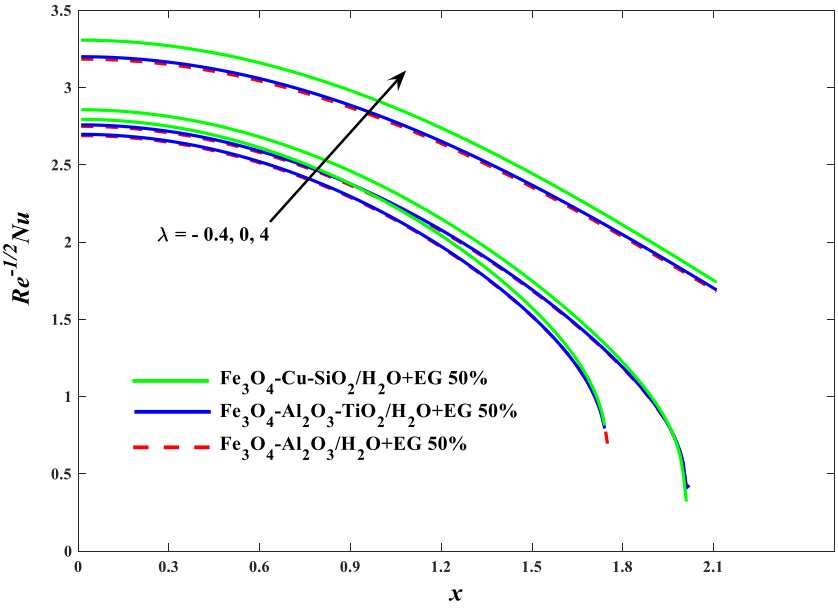

Fig. 5. $Re^{-1/2}Nu$ impression to λ influence, at $\chi_{ABC}= 0.03, M= 2$ and $K= 2$.

an augmentation in magnetic field intensity causes a curb in velocity due to the reinforcing of Lorentz force creation, which in turn reduces the rate of transferring energy. Fig. 3 illustrates the response of the Nusselt number to raising the volume fraction of nanoparticles while preserving the other factors' effects as constants. The Nusselt number shows a growing value as the volume fraction of nanosolids rises. It is a consequence of the fact that the volume fraction of nanoparticles contributes to the improvement of the thermal conductivity of the original fluid, which improves its ability to transfer energy.

Fig. 4 illustrates how the Nusselt number responds to the impact of the micropolar factor's increasing values. This behavior is attributed to changes in fluid viscosity and velocity profiles, in which an increase in the micropolar factor results in more pronounced microstructural effects within the fluid, exhibiting different viscosity and velocity profiles. These changes in viscosity and velocity profiles affect the thermal boundary layer near the solid sphere's surface. Altered profiles can result in reduced heat transfer rates and, consequently, a decrease in the Nusselt number. Fig. 5 depicts how the Nusselt number responds as the values of the combined convection factor increase. It is clearly visible that there is a direct relationship between the mixed convection parameter and the

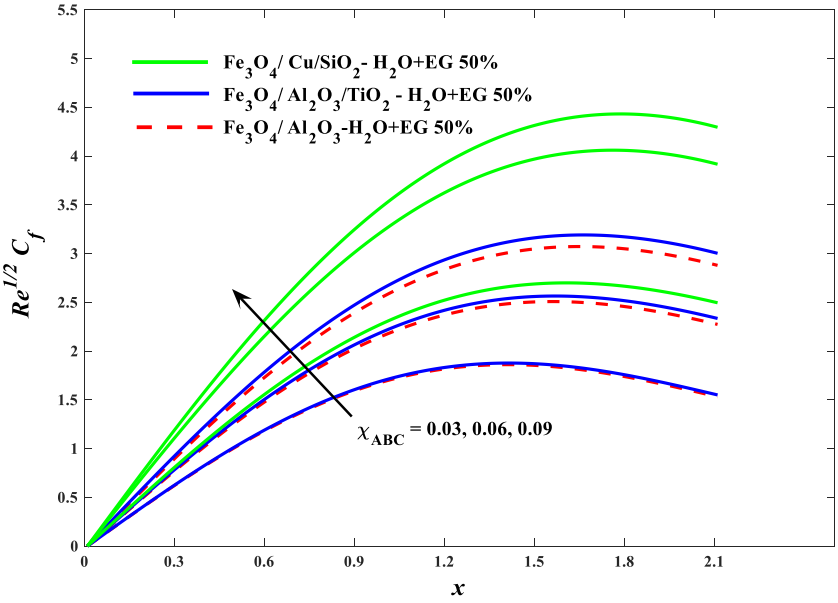

Fig. 6. $Re^{1/2}C_f$ impression to χ_{ABC} influence at M= 0.5, λ= 2 and K = 2.

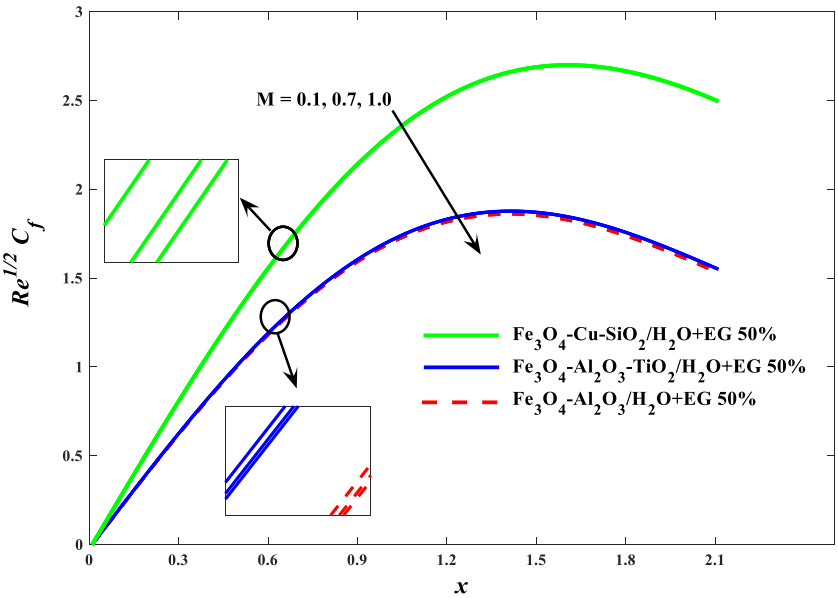

Fig. 7. $Re^{1/2}C_f$ impression to M influence at χ_{ABC}= 0.03, λ= 2 and K = 2.

Nusselt number. With a higher mixed convection factor, the buoyancy forces induced by temperature variations become more dominant. This results in stronger fluid motion driven by buoyancy, leading to an enhanced heat transfer rate. In Fig. 6, the skin friction takes on an increasing behavior when the volume fraction indicator values grow. The augmentation of the volume fraction factor leads to an elevation in shear stress at the interface between the fluid and the surface. This increase is accompanied by a rise in the fluid's viscosity, which further contributes to an escalation in skin friction. Fig. 7 demonstrates how skin friction tends to decline as the strength of the magnetic field increases. The magnetic field interacts with the moving charges within the fluid, generating a Lorentz force. The Lorentz force acts perpendicular to both the magnetic field and the fluid velocity. In the case of boundary layer flow on a sphere, this Lorentz force acts against the direction of flow, reducing the fluid movement near the surface of the sphere. In light of the inverse relationship between magnetic field strength and fluid movement, frictional forces are diminished. Fig. 8 shows that skin friction tends to rise along with the growth of the mixed convection factor. The observed behavior can be attributed to the influence of buoyancy factors. When the mixed convection factor grows, the significance of buoyancy forces becomes more pronounced. Buoyancy-driven flow tends to enhance the velocity gradients near the surface of the sphere, thereby causing an increase in skin friction. The

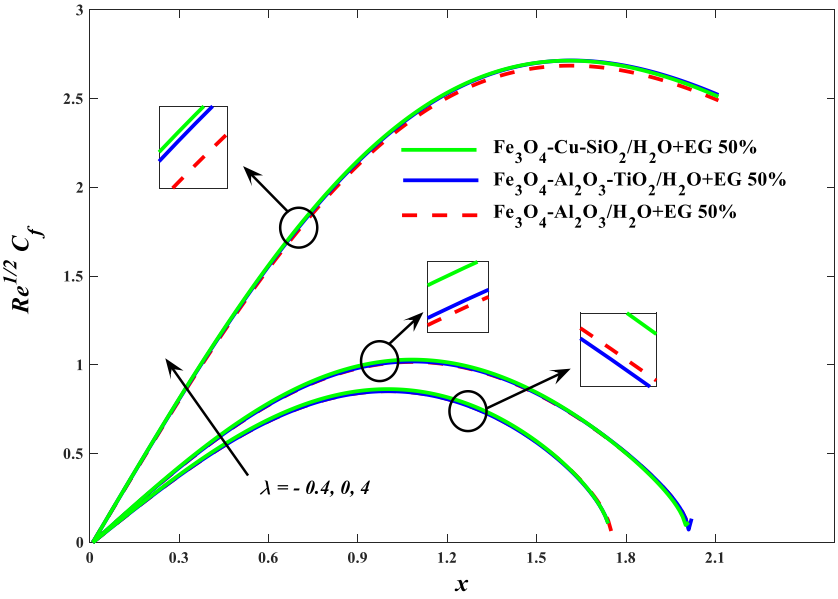

Fig. 8. $Re^{1/2}C_f$ impression to λ influence at $\chi_{ABC}= 0.03, M= 0.5$ and $K= 2$.

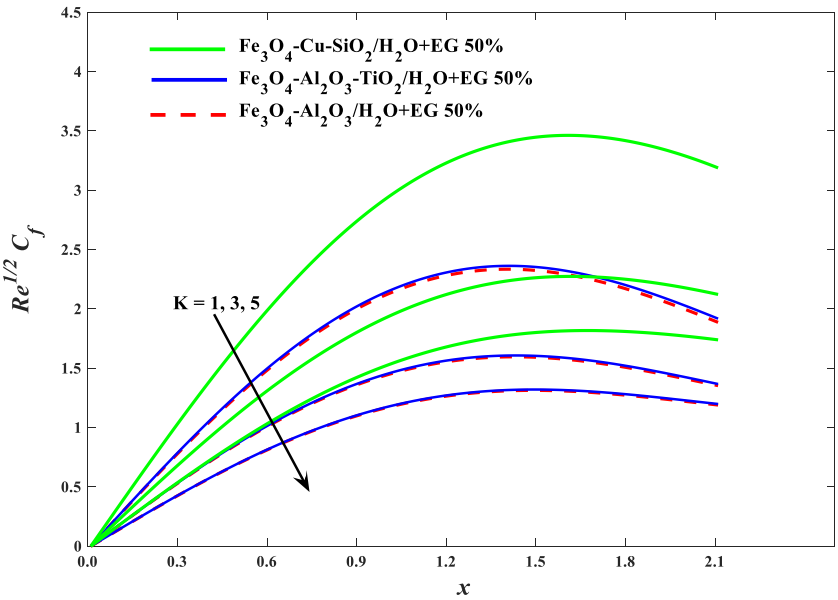

Fig. 9. $Re^{1/2}C_f$ impression to K influence at $\chi_{ABC}= 0.03, \lambda= 2$ and $M= 0.5$.

inverse response to skin friction upon increasing micropolar indicator values is clearly determined in Fig. 9. Increasing the micropolar factor in the boundary layer flow implies a stronger influence of microstructural rotations and microstructural resistance to deformation. These effects can lead to alterations in flow patterns, attenuation of shear stresses, and ultimately a decrease in skin friction. Furthermore, Figs. 2–9 show that tri-hybrid nanoparticles performed better than hybrid nanoparticles in terms of heat transport and skin friction. In comparison to Fe_3O_4–Al_2O_3–TiO_2, it is recommended to use Fe_3O_4–Cu–SiO_2 if we desire to transfer heat as efficiently as possible.

In Fig. 10, an augmentation in volume fraction contributes to an improvement in fluid velocity. By augmenting the volume fraction with small values recommended in previous studies, we ensure that the enhancement in buoyancy forces is higher than the viscosity forces, which leads to an improvement in the fluid velocity. It can be determined from Fig. 11 that, with the growth of the mixed convection indicator, the fluid's velocity tends to increase. It's commonly known that as the coefficient of mixed convection gets higher, the buoyancy forces also improve, resulting in an increase in fluid movement. Fig. 12 depicts the behavior of the velocity profiles when subjected to an intensifying magnetic field. Lorentz forces arise with the augmentation of the intensity of the magnetic

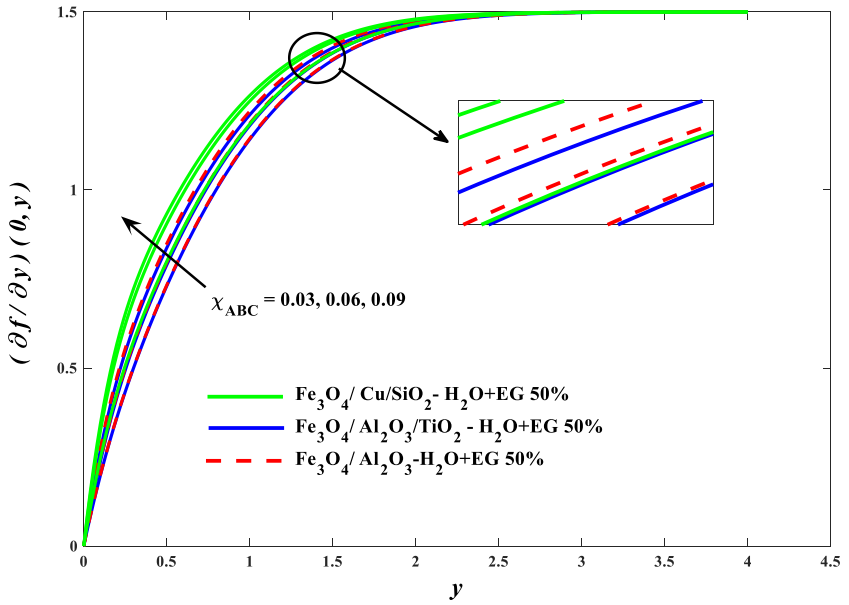

Fig. 10. Velocity impression to χ_{ABC} influence, at $M = 0.5, \lambda = 2$ and $K = 2$.

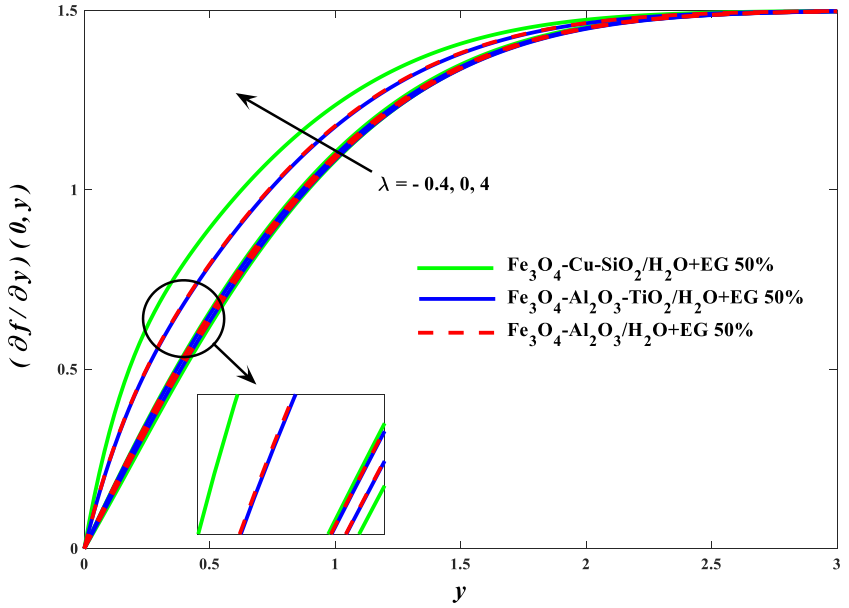

Fig. 11. Velocity impression to λ influence, at $\chi_{ABC} = 0.03, K = 2$ and $M = 0.5$.

force; these forces act against the movement of the fluid and slow down its velocity.

Fig. 13 shows how the velocity profiles respond to the increasing effects of the micropolar factor. It is obvious that as the micropolar factor tends to increase, the fluid velocity declines. As the micropolar parameter increases, the microstructural elements within the micropolar fluid introduce additional resistance and disrupt the flow near the surface of the sphere. This can result in a decrease in the overall fluid velocity. Fig. 14 identifies the effects of the growing magnetization factor on the temperature. It is observed that the escalating influence of the magnetic factor on temperatures is positive. By increasing the magnetic factor, the fluid's motion is suppressed, causing its temperature to rise. Fig. 15 depicts the temperature impact of increasing the combined convection indicator. The buoyant forces are significantly improved as the combined convection factor increases, causing the temperature profiles to decline. Impressions of temperature profiles with escalating volume fraction values are depicted in Fig. 16. The temperature profiles tend to rise at volume fraction values due to the improvement that will occur in the thermal conductivity of the host liquid. Fig. 17 is plotted to investigate the impact of the micropolar factor on the temperature. It is evident that raising the micropolar factor boosts the

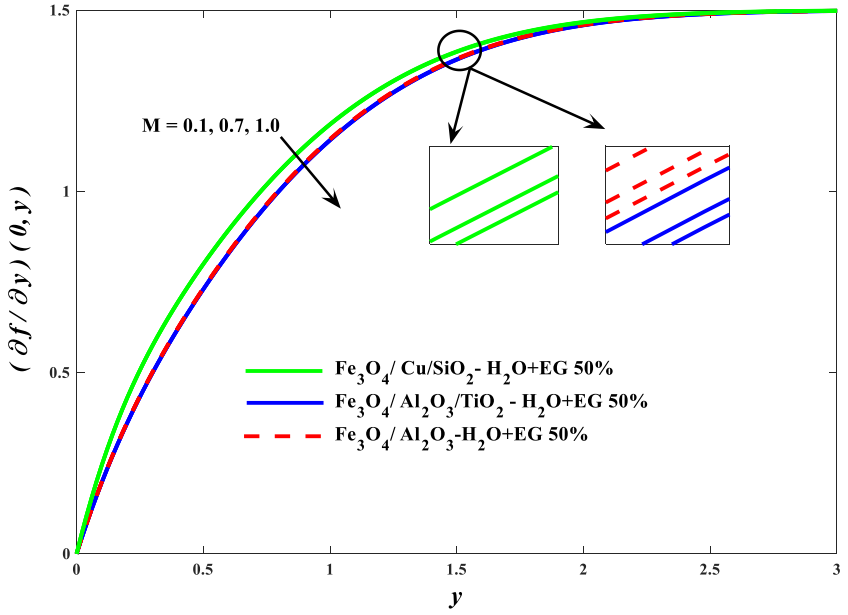

Fig. 12. Velocity impression to M influence, at $\chi_{ABC}= 0.03, \lambda= 2$ and $K= 2$.

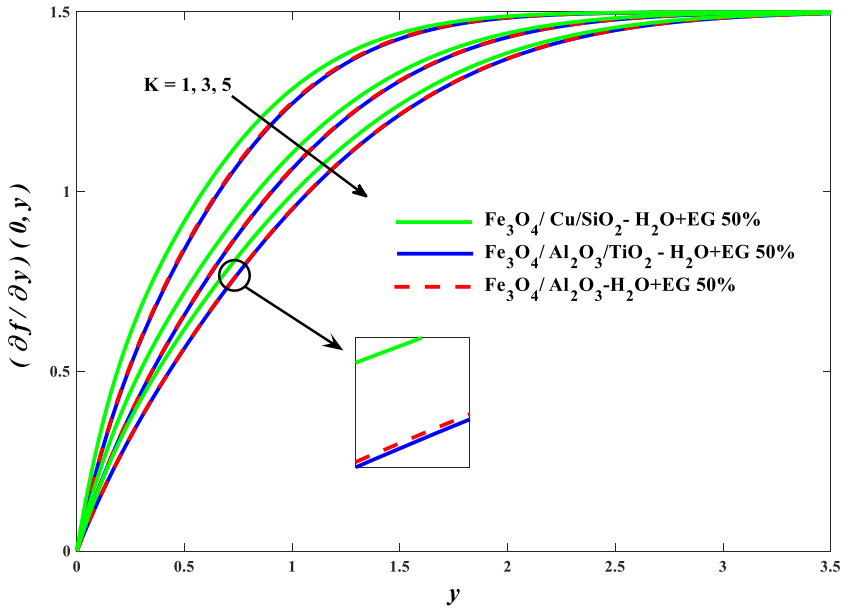

Fig. 13. Velocity impression to K influence, at $\chi_{ABC}= 0.03, \lambda= 2$ and $M= 0.5$.

temperature. This response could be explained by increasing the micropolar factor, which also enhances the viscous forces.

From Fig. 18, it can be observed that when the magnetic field strength increases, the angular velocity tends to decrease. The Lorentz force, whose creation is promoted by the passage of a magnetic field through a liquid in motion, is responsible for these patterns of behavior. Fig. 19 depicts how the angular velocity responds to increasing volume fraction values. When its values go up, the response of the angular velocity profiles is positive. Normally, higher values of the volume fraction improve the thermal conductivity of the base fluid, which leads to an enhancement of the angular velocity. Fig. 20 depicts how the angular velocity changes with growing micropolar factor values. As their values rise, the angular velocity profiles tend to decline. This is because increasing the polar factor improves the nanofluid's viscosity. Fig. 21 displays the relationship between the mixed convection factor and the angular velocity. It is clear that there is a positive relationship between them. As mentioned earlier, the increase in the combined convection factor improves the buoyancy forces, which ensures an increase in the angular velocity.

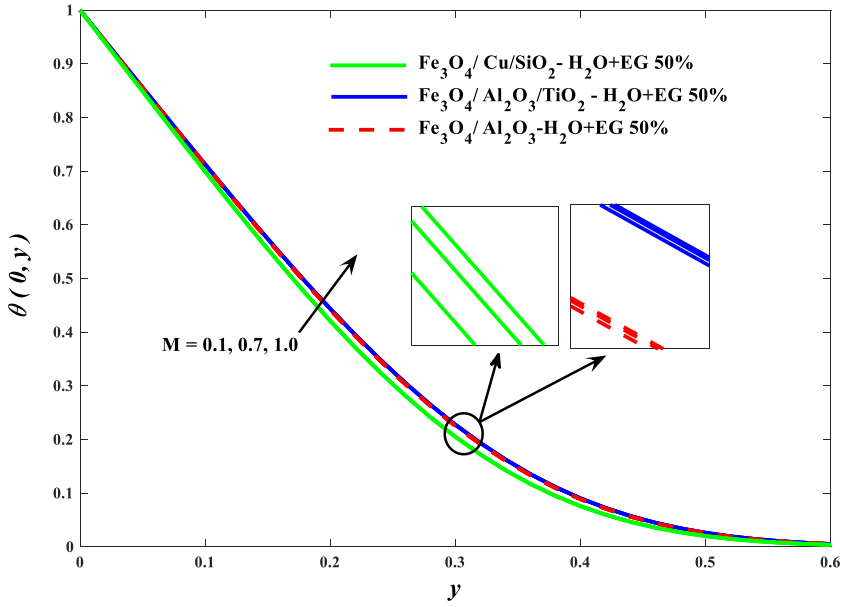

Fig. 14. Temperature impression to M influence, at $\chi_{ABC}= 0.03, \lambda= 2$ and $K= 2$.

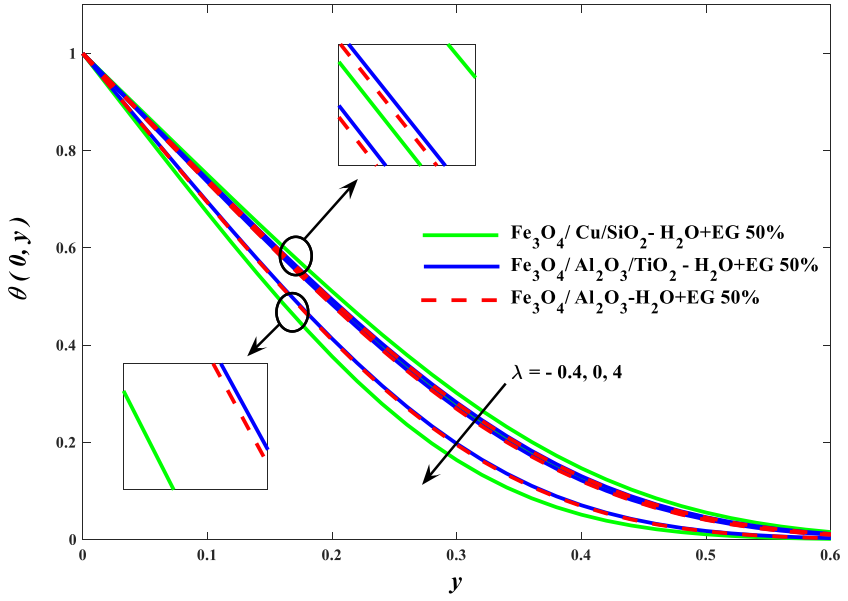

Fig. 15. Temperature impression to λ influence, at $\chi_{ABC}= 0.03, K= 2$ and $M= 0.5$.

5. Conclusion

The combined convection energy transport characteristics of magnetized ferro-ternary hybrid-nanofluid moving around a spherical object has been simulated in this article along with the micropolar model. The foremost objective is to create a visualization of the effects of non-dimensional factors such as combined convection, magnetism, micropolar, and volume fraction factors. Numerical findings for various factor conditions were obtained graphically in terms of skin friction, Nusselt number, angular velocity, velocity, and temperature at a spherical surface and discussed from a physical standpoint. Analyzing the results of the research, the following conclusions can be drawn:

- Ternary hybrid nanosolids are extremely advantageous for improving both flow perspectives and convective energy transport.

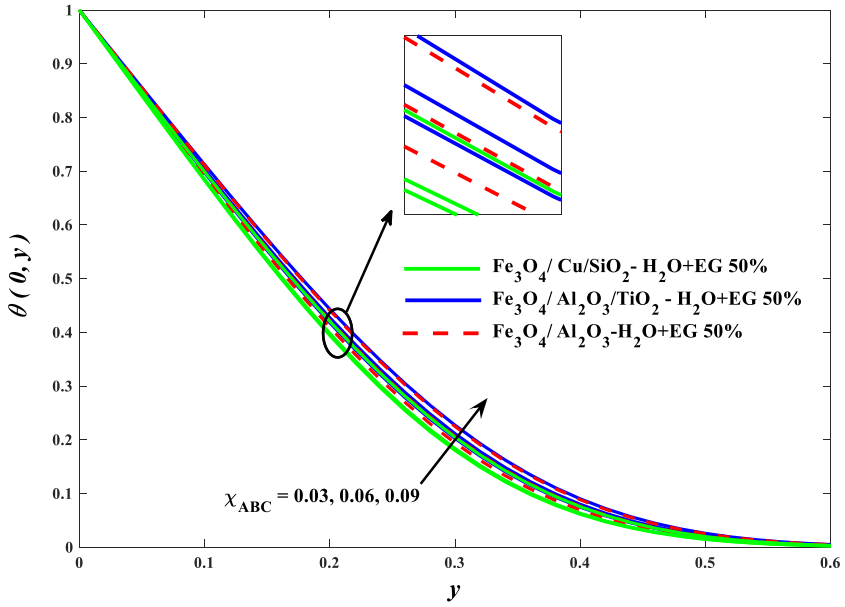

Fig. 16. Temperature impression to χ_{ABC} influence, at $M = 0.5, \lambda = 2$ and $K = 2$.

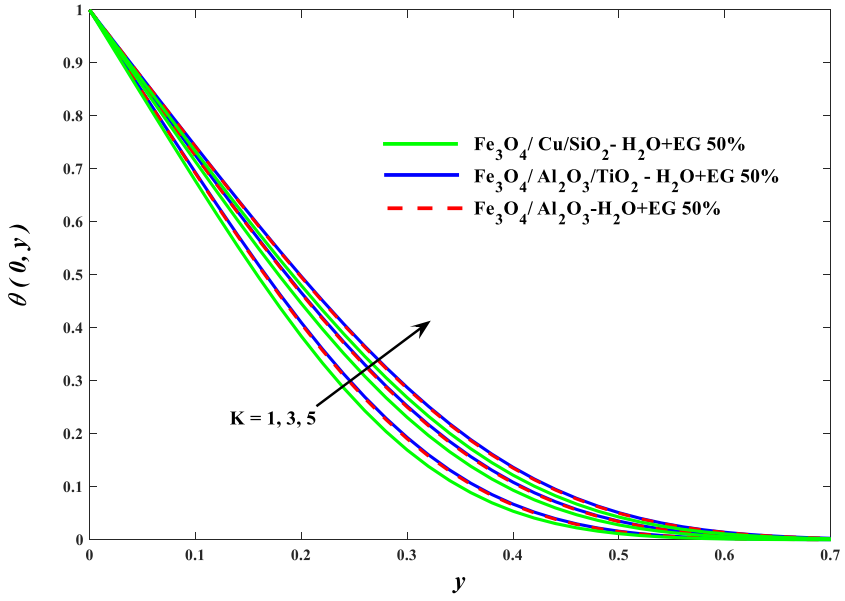

Fig. 17. Temperature impression K influence, $\chi_{ABC} = 0.03, \lambda = 2$ and $M = 0.5$.

- A higher value of the volume fraction of ternary hybrid nonsolid has produced an optimization of Nusselt number, velocity, and temperature.
- The Lorentz forces have the ability to suppress the flow strength, skin friction, and rate at which energy is transferred.
- The micropolar factor has a similar effect on the studied physical groups as the Lorentz forces, but with less intensity.
- The mixed convection factor essentially contributes to higher levels of energy transfer and better flow scenarios.
- In comparison to Fe_3O_4–Al_2O_3–TiO_2, it is recommended to use Fe_3O_4–Cu–SiO_2 if we desire to transfer heat as efficiently as possible.

Depending on this research, we can consider some future studies. The present problem can be extended in future investigations employing more additional physical impacts, such as thermal radiation, chemical reactions, viscous dissipation, and joule heating effects, as well as ternary hybrid nanofluids with viscous dissipation and joule heating impacts. Additionally, it can employ other boundary conditions, such as convective boundary conditions, constant heat flux, etc.

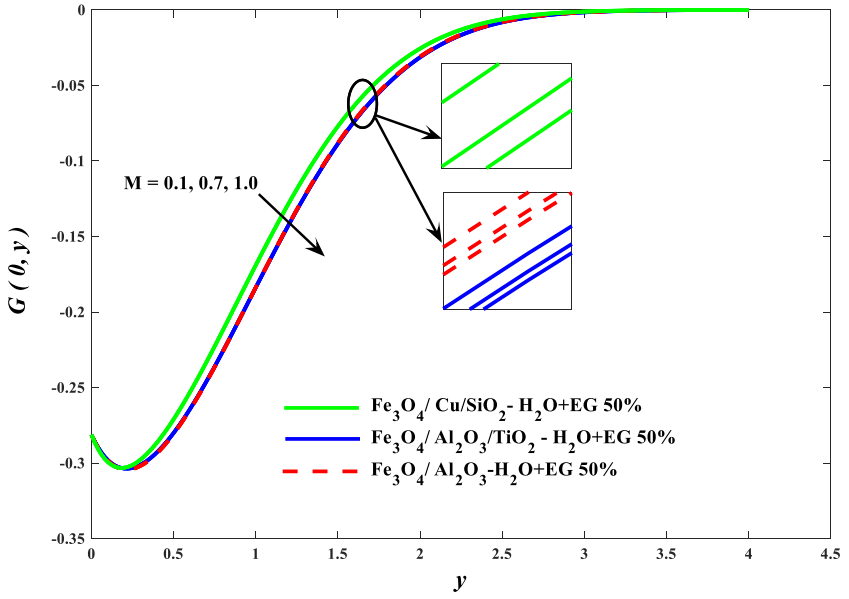

Fig. 18. Angular velocity impression to M influence, at $\chi_{ABC}= 0.03, \lambda= 2$ and $K= 2$.

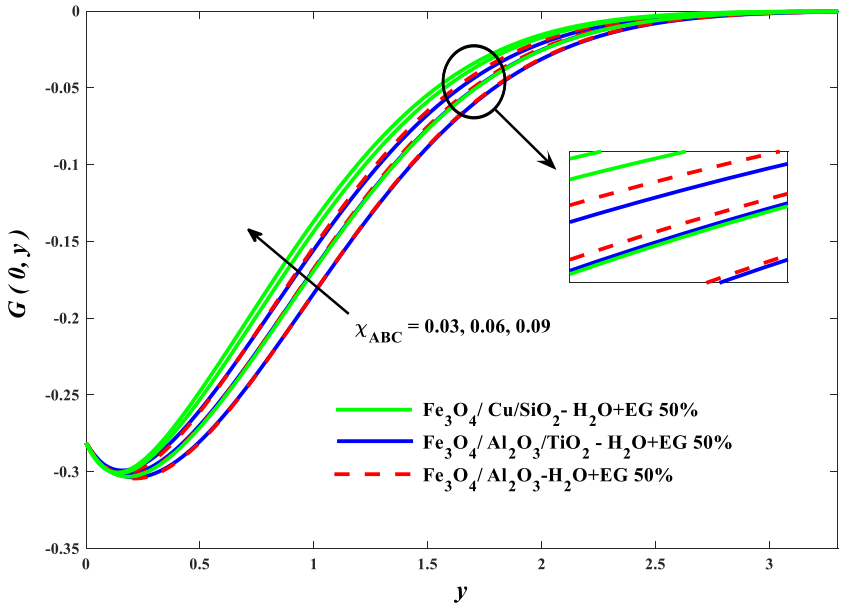

Fig. 19. Angular velocity impression to χ_{ABC} influence, at $M= 0.5, \lambda= 2$ and $K= 2$.

CRediT authorship contribution statement

Mohammed Z. Swalmeh: Conceptualization, Formal analysis, Investigation, Methodology, Software, Visualization, Writing – original draft, Writing – review & editing, Validation. **Firas A. Alwawi:** Investigation, Methodology, Validation, Writing – original draft, Writing – review & editing. **A.A. Altawallbeh:** Formal analysis, Investigation, Methodology, Software, Writing – original draft, Writing – review & editing. **Kohilavani Naganthran:** Formal analysis, Funding acquisition, Project administration, Software, Writing – original draft, Writing – review & editing. **Ishak Hashim:** Investigation, Resources, Supervision, Visualization, Writing – original draft, Writing – review & editing.

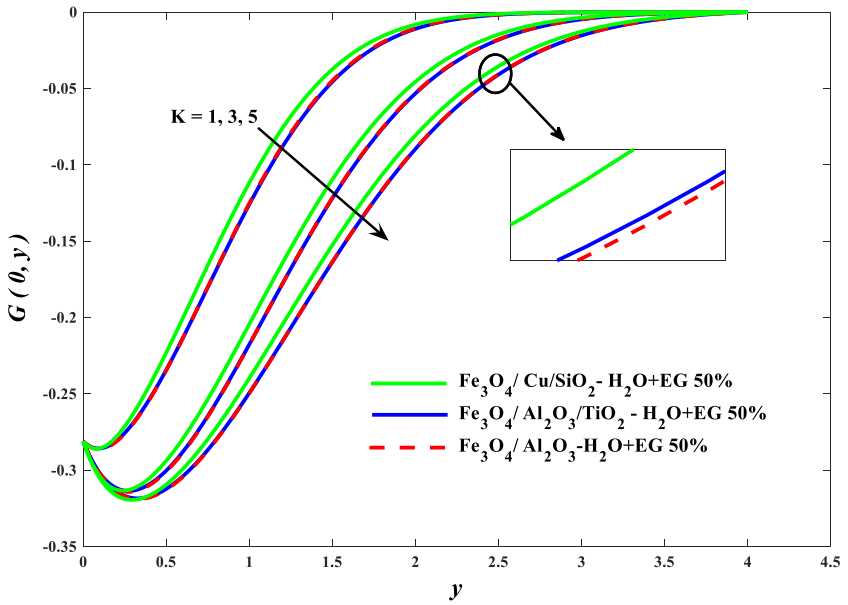

Fig. 20. Angular velocity impression to K influence, at $\chi_{ABC}= 0.01, \lambda= 2$ and $M= 0.5$.

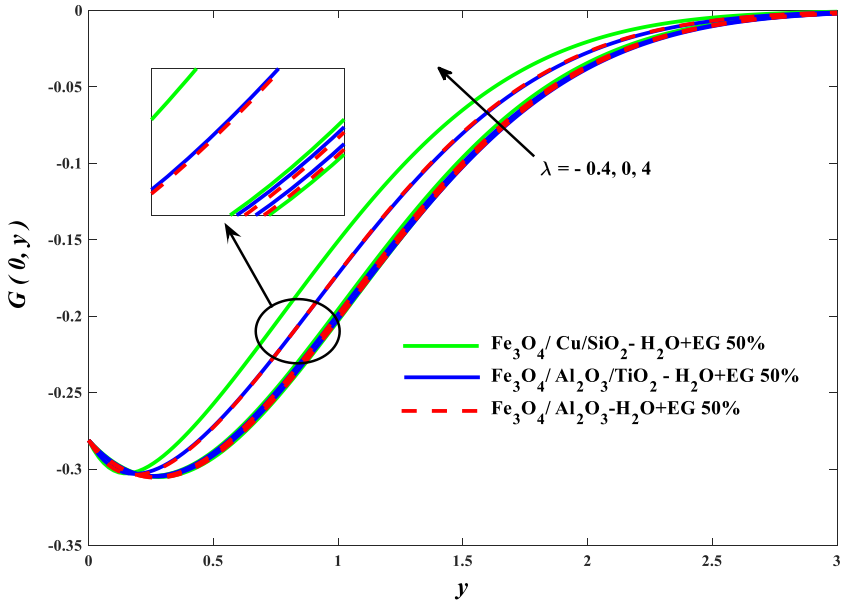

Fig. 21. Angular velocity impression to λ influence at $\chi_{ABC}= 0.03, K= 2$ and $M= 0.5$.

Declaration of competing interest

The authors declare that they have no known competing financial interests or personal relationships that could have appeared to influence the work reported in this paper.

Acknowledgment

K.N. would like to acknowledge the grant RMF1965-2021 received from Universiti Malaya.

Nomenclature

a	Radius of sphere (m)
B_0	Magnetic field strength (kg /s^{2}A)
C_f	Skin friction
G	Angular velocity (rad/s)
Gr	Grashof number
g	Gravity vector
K	Micropolar factor
k	Thermal conductivity (W /mK)
M	Magnetic parameter
Nu	Nusselt Number
Pr	Prandtl number
Re	Reynolds number
T	Temperature of the fluid (K)
T_w	Wall temperature (K)

Subscript

f	Original liquid
nf	Nanoliquid
T_∞	Ambient temperature (K)
$v\ x$	component of velocity (m /s)
$w\ y$	component of velocity (m /s)
ν_f	Kinematic viscosity (m^2 /s)
v_e	Velocity of external flow (m /s)
U_∞	Free stream velocity (m /s)
χ	Volume fraction factor
κ	Vortex viscosity (N·s/m^2)
μ	Dynamic viscosity (kg/m s)
ρ	Density (kg/m^3)
σ	Electrical conductivity (S /m)
β	Thermal expansion coefficient (K^{-1})
χ	Volume fraction factor
hnf	Hybrid nanoliquid
$thnf$	Ternary hybrid nanoliquid

References

[1] A.C. Eringen, Simple microfluids, Int. J. Eng. Sci. 2 (2) (1964) 205–217.
[2] A.C. Eringen, Theory of micropolar fluids, J. Mathemat. Mechanics (1966) 1–18.
[3] R. Nazar, N. Amin, I. Pop, Mixed convection boundary layer flow about an isothermal sphere in a micropolar fluid, Int. J. Therm. Sci. 42 (3) (2003) 283–293.
[4] R. Nazar, N. Amin, T. Groşan, I. Pop, Free convection boundary layer on a sphere with constant surface heat flux in a micropolar fluid, Int. Commun. Heat Mass Tran. 29 (8) (2002) 1129–1138.
[5] R. Nazar, N. Amin, Free convection boundary layer on an isothermal sphere in a micropolar fluid, Int. Commun. Heat Mass Tran. 29 (3) (2002) 377–386.
[6] C.-Y. Cheng, Natural convection heat and mass transfer from a sphere in micropolar fluids with constant wall temperature and concentration, Int. Commun. Heat Mass Tran. 35 (6) (2008) 750–755.
[7] M. Salleh, R. Nazar, I. Pop, Numerical solutions of free convection boundary layer flow on a solid sphere with Newtonian heating in a micropolar fluid, Meccanica 47 (5) (2012) 1261–1269.
[8] N.C. Roy, M.A. Hossain, Unsteady magnetohydrodynamic mixed convection flow of micropolar fluid past a permeable sphere, J. Thermophys. Heat Tran. 31 (3) (2017) 686–699.
[9] M.Z. Swalmeh, H.T. Alkasasbeh, A. Hussanan, M. Mamat, Heat transfer flow of Cu-water and Al_2O_3-water micropolar nanofluids about a solid sphere in the presence of natural convection using Keller-box method, Res. Phys. 9 (2018) 717–724.
[10] H.A. Alzgool, H.T. Alkasasbeh, S. Abu-ghurra, Z. Al-houri, M.Z. Swalmeh, Numerical solution of heat transfer in MHD mixed convection flow micropolar Casson fluid about solid sphere with radiation effect, Int. J. Eng. Res. Technol. 12 (4) (2019) 519–529.
[11] S. EL-Kabeir, A. Rashad, W. Khan, Z.M. Abdelrahman, Micropolar ferrofluid flow via natural convective about a radiative isoflux sphere, Adv. Mech. Eng. 13 (2) (2021), 1687814021994392.
[12] S.U. Choi, J.A. Eastman, Enhancing Thermal Conductivity of Fluids with Nanoparticles, Argonne National Lab.(ANL), Argonne, IL (United States), 1995.
[13] E.I. Cherecheş, J.I. Prado, M. Cherecheş, A.A. Minea, L. Lugo, Experimental study on thermophysical properties of alumina nanoparticle enhanced ionic liquids, J. Mol. Liq. 291 (2019), 111332.
[14] R.K. Das, G.S. Sokhal, S.S. Sehgal, A numerical study on the performance of water based copper oxide nanofluids in compact channel, Mater. Today: Proc. 33 (2020) 1499–1504.
[15] A.A. Minea, P. Estellé, Numerical study on CNT nanofluids behavior in laminar pipe flow, J. Mol. Liq. 271 (2018) 281–289.
[16] S.S. Murshed, P. Estellé, A state of the art review on viscosity of nanofluids, Renew. Sustain. Energy Rev. 76 (2017) 1134–1152.

[17] S. Saleem, I. Animasaun, S.-J. Yook, Q.M. Al-Mdallal, N.A. Shah, M. Faisal, Insight into the motion of water conveying three kinds of nanoparticles shapes on a horizontal surface: significance of thermo-migration and Brownian motion, Surface. Interfac. 30 (2022), 101854.

[18] J. Gil-Font, et al., Improving heat transfer of stabilised thermal oil-based tin nanofluids using biosurfactant and molecular layer deposition, Appl. Therm. Eng. 178 (2020), 115559.

[19] H.E. Patel, T. Sundararajan, S.K. Das, An experimental investigation into the thermal conductivity enhancement in oxide and metallic nanofluids, J. Nano Res. 12 (3) (2010) 1015–1031.

[20] A. Sofiah, M. Samykano, A. Pandey, K. Kadirgama, K. Sharma, R. Saidur, Immense impact from small particles: review on stability and thermophysical properties of nanofluids, Sustain. Energy Technol. Assessments 48 (2021), 101635.

[21] S. Nasir, Z. Shah, S. Islam, E. Bonyah, T. Gul, Darcy Forchheimer nanofluid thin film flow of SWCNTs and heat transfer analysis over an unsteady stretching sheet, AIP Adv. 9 (1) (2019).

[22] R. Turcu, et al., New polypyrrole-multiwall carbon nanotubes hybrid materials, J. Optoelectron. Adv. Mater. 8 (2) (2006) 643–647.

[23] S. Suresh, K. Venkitaraj, P. Selvakumar, M. Chandrasekar, Synthesis of Al_2O_3–Cu/water hybrid nanofluids using two step method and its thermo physical properties, Colloids Surf. A Physicochem. Eng. Asp. 388 (1–3) (2011) 41–48.

[24] M. Baghbanzadeh, A. Rashidi, D. Rashtchian, R. Lotfi, A. Amrollahi, Synthesis of spherical silica/multiwall carbon nanotubes hybrid nanostructures and investigation of thermal conductivity of related nanofluids, Thermochim. Acta 549 (2012) 87–94.

[25] M. Muneeshwaran, G. Srinivasan, P. Muthukumar, C.-C. Wang, Role of hybrid-nanofluid in heat transfer enhancement–A review, Int. Commun. Heat Mass Tran. 125 (2021), 105341.

[26] A. Jamaludin, K. Naganthran, R. Nazar, I. Pop, MHD mixed convection stagnation-point flow of Cu-Al_2O_3/water hybrid nanofluid over a permeable stretching/shrinking surface with heat source/sink, Eur. J. Mech. B Fluid 84 (2020) 71–80.

[27] S. Nasir, A.S. Berrouk, A. Aamir, T. Gul, I. Ali, Features of flow and heat transport of MoS_2+ GO hybrid nanofluid with nonlinear chemical reaction, radiation and energy source around a whirling sphere, Heliyon 9 (4) (2023).

[28] E.H. Aly, A.V. Roşca, N.C. Roşca, I. Pop, Convective heat transfer of a hybrid nanofluid over a nonlinearly stretching surface with radiation effect, Mathematics 9 (18) (2021) 2220.

[29] F.A. Alwawi, F.M. Al Faqih, M.Z. Swalmeh, M.A.H. Ibrahim, Combined convective energy transmission performance of Williamson hybrid nanofluid over a cylindrical shape with magnetic and radiation impressions, Mathematics 10 (17) (2022) 3191.

[30] F.A. Alwawi, M.Z. Swalmeh, A.S. Qazaq, R. Idris, Heat transmission reinforcers induced by MHD hybrid nanoparticles for water/water-EG flowing over a cylinder, Coatings 11 (6) (2021) 623.

[31] P. Rana, G. Gupta, FEM Solution to quadratic convective and radiative flow of Ag-MgO/H_2O hybrid nanofluid over a rotating cone with Hall current: optimization using Response Surface Methodology, Math. Comput. Simulat. 201 (2022) 121–140.

[32] P. Patil, B. Goudar, Time-dependent mixed convection flow of Ag–MgO/water hybrid nanofluid over a moving vertical cone with rough surface, J. Therm. Anal. Calorim. (2022) 1–13.

[33] F. Alwawi, M. Swalmeh, I. Sulaiman, N. Yaseen, H. Alkasasbeh, T. Al Soub, Numerical investigation of heat transfer characteristics for blood/water-based hybrid nanofluids in free convection about a circular cylinder, J. Mech. Eng. Sci. 16 (2) (2022) 8931–8942.

[34] O.A.S. Alzu'bi, F.A. Alwawi, M.Z. Swalmeh, I.M. Sulaiman, A.S. Hamarsheh, M.A.H. Ibrahim, Energy transfer through a magnetized Williamson hybrid nanofluid flowing around a spherical surface: numerical simulation, Mathematics 10 (20) (2022) 3823.

[35] M.Z. Swalmeh, et al., Numerical simulation on energy transfer enhancement of a Williamson ferrofluid subjected to thermal radiation and a magnetic field using hybrid ultrafine particles, Sci. Rep. 13 (1) (2023) 3176.

[36] T. Gul, et al., Simulation of the water-based hybrid nanofluids flow through a porous cavity for the applications of the heat transfer, Sci. Rep. 13 (1) (2023) 7009.

[37] H. Adun, D. Kavaz, M. Dagbasi, Review of ternary hybrid nanofluid: synthesis, stability, thermophysical properties, heat transfer applications, and environmental effects, J. Clean. Prod. 328 (2021), 129525.

[38] R. Rekha Sahoo, Effect of various shape and nanoparticle concentration based ternary hybrid nanofluid coolant on the thermal performance for automotive radiator, Heat Mass Tran. 57 (5) (2021) 873–887.

[39] V. Kumar, R.R. Sahoo, Experimental and numerical study on cooling system waste heat recovery for engine air preheating by ternary hybrid nanofluid, J. Enhanc. Heat Transf. 28 (4) (2021).

[40] A. Dezfulizadeh, A. Aghaei, A. Hassani Joshaghani, M.M. Najafizadeh, Exergy efficiency of a novel heat exchanger under MHD effects filled with water-based Cu–SiO_2-MWCNT ternary hybrid nanofluid based on empirical data, J. Therm. Anal. Calorim. 147 (7) (2022) 4781–4804.

[41] U. Khan, Z. Mahmood, MHD Stagnation Point Flow of Ternary Hybrid Nanofluid Flow over a Stretching/shrinking Cylinder with Suction and Ohmic Heating, 2022.

[42] S. Manjunatha, V. Puneeth, B. Gireesha, A. Chamkha, Theoretical study of convective heat transfer in ternary nanofluid flowing past a stretching sheet, J. Appl. Computat. Mechan. 8 (4) (2022) 1279–1286.

[43] E.A. Algehyne, et al., Thermal improvement in pseudo-plastic material using ternary hybrid nanoparticles via non-Fourier's law over porous heated surface, Energies 14 (23) (2021) 8115.

[44] I. Animasaun, S.-J. Yook, T. Muhammad, A. Mathew, Dynamics of ternary-hybrid nanofluid subject to magnetic flux density and heat source or sink on a convectively heated surface, Surface. Interfac. 28 (2022), 101654.

[45] S. Nasir, S. Sirisubtawee, N. Akkurt, I. Ali, T. Gul, P. Juntharee, Simultaneous features of ternary hybrid nanoparticles on thermal radiative flow configured by Darcy–Forchheimer porous surface, Int. J. Mod. Phys. B (2023), 2450015.

[46] A.S. Alnahdi, S. Nasir, T. Gul, Ternary Casson hybrid nanofluids in convergent/divergent channel for the application of medication, Therm. Sci. 27 (2023) 67–76. Spec. issue 1.

[47] S. Nasir, S. Sirisubtawee, P. Juntharee, A.S. Berrouk, S. Mukhtar, T. Gul, Heat transport study of ternary hybrid nanofluid flow under magnetic dipole together with nonlinear thermal radiation, Appl. Nanosci. 12 (9) (2022) 2777–2788.

[48] S. Nasir, A.S. Berrouk, A. Aamir, T. Gul, Significance of chemical reactions and entropy on Darcy-forchheimer flow of H2O and C2H6O2 convening magnetized nanoparticles, Int. J. Thermofluids 17 (2023), 100265.

[49] T. Sreelakshmi, A. Annamma, A. Chethan, M. Krishna Murthy, C. Raju, Nonlinear thermal buoyancy on ferromagnetic liquid stream over a radiated elastic surface with non fourier heat flux, Comput. Model. Eng. Sci. 126 (2) (2021) 599–616.

[50] M. Ramzan, S. Rehman, M.S. Junaid, A. Saeed, P. Kumam, W. Watthayu, Dynamics of Williamson Ferro-nanofluid due to bioconvection in the portfolio of magnetic dipole and activation energy over a stretching sheet, Int. Commun. Heat Mass Tran. 137 (2022), 106245.

[51] L. Boutina, R. Bessaïh, Numerical simulation of mixed convection air-cooling of electronic components mounted in an inclined channel, Appl. Therm. Eng. 31 (11–12) (2011) 2052–2062.

[52] O.A. Bég, A. Bakier, R. Prasad, S.K. Ghosh, Numerical modelling of non-similar mixed convection heat and species transfer along an inclined solar energy collector surface with cross diffusion effects, World J. Mech. 2011 (2011).

[53] S. Nasir, et al., Three-dimensional rotating flow of MHD single wall carbon nanotubes over a stretching sheet in presence of thermal radiation, Appl. Nanosci. 8 (2018) 1361–1378.

[54] A.S. Alsagri, et al., MHD thin film flow and thermal analysis of blood with CNTs nanofluid, Coatings 9 (3) (2019) 175.

[55] S. Nasir, A.S. Berrouk, T. Gul, I. Zari, W. Alghamdi, I. Ali, Unsteady mix convectional stagnation point flow of nanofluid over a movable electro-magnetohydrodynamics Riga plate numerical approach, Sci. Rep. 13 (1) (2023), 10947.

[56] M.Z. Swalmeh, et al., Effectiveness of radiation on magneto-combined convective boundary layer flow in polar nanofluid around a spherical shape, Fractal and Fractional 6 (7) (2022) 383.

[57] F.A. Alwawi, A.S. Hamarsheh, H.T. Alkasasbeh, R. Idris, Mixed convection flow of magnetized Casson nanofluid over a cylindrical surface, Coatings 12 (3) (2022) 296.
[58] M.K.A. Mohamed, N.A.Z.M. Noar, M.Z. Salleh, A. Ishak, Free convection boundary layer flow on a solid sphere in a nanofluid with viscous dissipation, Malaysian J. Fundamental Appl. Sci. 15 (3) (2019) 381–388.
[59] S. Karthikeyan, G.R. Solomon, V. Kumaresan, R. Velraj, Parametric studies on packed bed storage unit filled with PCM encapsulated spherical containers for low temperature solar air heating applications, Energy Convers. Manag. 78 (2014) 74–80.
[60] S. Sachdev, S. Pareek, B. Mahadevan, A. Deshpande, Modeling and simulation of single phase fluid flow and heat transfer in packed beds, in: Excerpt from the Proceedings of the 2012 COMSOL Conference in Bangalore, 2012.
[61] M. Shamshuddin, N. Akkurt, A. Saeed, P. Kumam, Radiation mechanism on dissipative ternary hybrid nanoliquid flow through rotating disk encountered by Hall currents: HAM solution, Alex. Eng. J. 65 (2023) 543–559.
[62] F.A. Alwawi, N. Yaseen, M.Z. Swalmeh, A.S. Qazaq, A computational numerical simulation of free convection catalysts for magnetized micropolar ethylene glycol via copper and graphene oxide nanosolids, Proc. IME E J. Process Mech. Eng. (2022), 09544089221146157.
[63] M. Swalmeh, H. Alkasasbeh, A. Hussanan, M. Mamat, Numerical study of mixed convection heat transfer in methanol based micropolar nanofluid about a horizontal circular cylinder, J. Phys. Conf. 1366 (1) (2019), 012003. IOP Publishing.
[64] F.A. Alwawi, M.Z. Swalmeh, A.S. Hamarsheh, Computational simulation and parametric analysis of the effectiveness of ternary nano-composites in improving magneto-micropolar liquid heat transport performance, Symmetry 15 (2) (2023) 429.
[65] T. Cebeci, P. Bradshaw, Physical and Computational Aspects of Convective Heat Transfer, Springer Science & Business Media, 2012.
[66] F. Alwawi, I.M. Sulaiman, M.Z. Swalmeh, N. Yaseen, Energy transport boosters of magneto micropolar fluid flowing past a cylinder: a case of laminar combined convection, Proc. Inst. Mech. Eng. C. J. Mech. Eng. Sci. 236 (22) (2022) 10902–10913.
[67] N. Yaseen, F. Shatat, F.A. Alwawi, M.Z. Swalmeh, M.S. Kausar, I.M. Sulaiman, Using micropolar nanofluid under a magnetic field to enhance natural convective heat transfer around a spherical body, J. Adv. Res. Fluid Mech. Therm. Sci. 96 (1) (2022) 179–193.